Polymer Bulletin (2022) 79:4031–4048
https://doi.org/10.1007/s00289-021-03681-2

ORIGINAL PAPER

The effect of ZnO nanoparticles as Ag-carrier in PBAT for antimicrobial films

Alana G. de Souza[1] · Luiz Gustavo H. Komatsu[2] · Rennan F. S. Barbosa[1] · Duclerc F. Parra[2] · Derval S. Rosa[1]

Received: 10 January 2021 / Revised: 23 March 2021 / Accepted: 25 March 2021 /
Published online: 19 April 2021

Abstract

Zinc oxide (ZnO) and ZnO-silver (ZnO-Ag) nanoparticles (NPs) are widely used in different fields, such as biomedicine and food packaging, due to their recognized antibacterial activity and safety for human health. In this paper, ZnO and ZnO-Ag NPs were incorporated into poly(butylene adipate-co-terephthalate) (PBAT), in two contents (0.5 and 1 wt%), to prepare antibacterial films. The NPs were characterized by TEM and FT-Raman, and the films were analyzed by FT-Raman and FTIR, mechanical properties, SEM–EDS, TGA, DSC, XRD, and antibacterial properties against *Escherichia coli.* The results indicate that both NPs were physically retained in the polymer structure, with a strong electrostatic interaction between the mixture components, reflecting excellent mechanical behavior. The films showed good thermal stability, without significant changes, and the nanocomposites enhanced PBAT crystallinity from 18 to 23% and 27% for PBAT-ZnO and PBAT-ZnO-Ag films, respectively. The mechanical, thermal, and crystallinity results indicated the excellent potential of NPs in biodegradable films to improve properties and expand applicability. The antimicrobial activity is higher for PBAT-ZnO-Ag films than the pristine PBAT due to the synergic effect between the NPs and the oxidation–reduction potential of each nanoparticle, where the ZnO protect and stabilized the Ag-NPs, acting as an Ag-carrier, enhancing its antimicrobial effects after the film's preparation and allowing its applicability in biomedical products or food packaging.

✉ Derval S. Rosa
dervalrosa@yahoo.com.br

[1] Centro de Engenharia, Modelagem e Ciências Sociais Aplicadas–CECS/ Universidade Federal do ABC (UFABC), Avenida dos Estados, 5001, Santo André, SP CEP 09210-580, Brazil

[2] Instituto de pesquisas Energéticas e Nucleares–IPEN/CNEN, Av. Prof. Lineu Prestes, Cid Universitária, 2242, São Paulo, SP CEP 05508000, Brazil

Graphic abstract

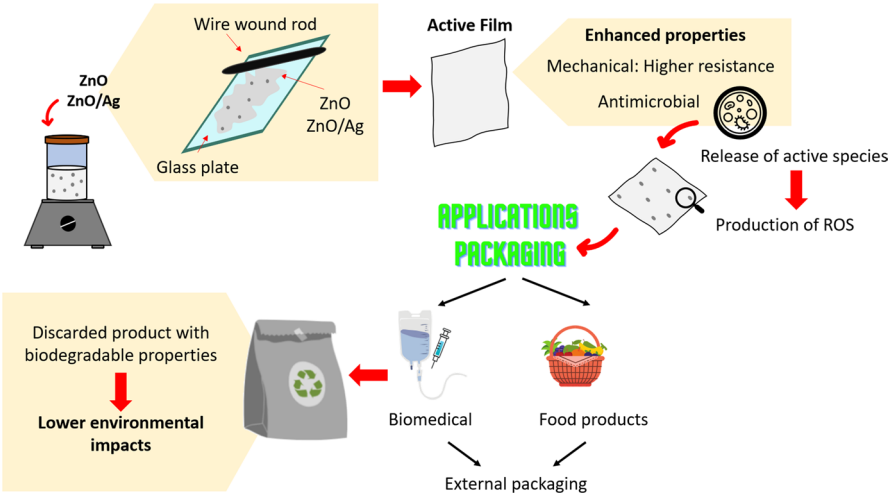

Keywords Zinc oxide nanoparticles · ZnO-Ag nanoparticles · PBAT nanocomposites · Antimicrobial activity · *E. coli*

Introduction

The interest in biopolymers and synthetic polymers with biodegradable characteristics has been rapidly increasing due to the growing environmental concerns associated with searching for new solutions to avoid the accumulation of materials as waste. There has been a trend in several industrial sectors in the last decade to replace the commodity plastics currently used, such as polypropylene and polyethylene, with biodegradable polymers [1–3].

PBAT is an aliphatic–aromatic polyester, completely biodegradable, synthesized from 1,4-butanediol, adipic acid, and terephthalic acid. It is a synthetic polymer that has high elongation at break and is very flexible. This polymer degrades in a few weeks in appropriate conditions and is processable with different methods [4]. However, the PBAT has no antimicrobial properties, and due to its chemical structure, it is easily attacked by microorganisms. Extensive research has been occurred to increase the PBAT film's functionality, mainly increasing the antimicrobial characteristics. The main applications are food packaging and medical-care facilities, and the biological activity allows this class of films to reduce, inhibit, or retard the growth of microorganisms present in the packed product [2, 5–7].

Innumerous active species can be used to promote biocidal properties, such as plant-derived natural extracts, chemicals, antibiotics, inorganic metal, and metal oxide ions [8–12]. Some metals and metal oxides nanoparticles (NPs) are considered safe and biocompatible, which allows the use in different packaging or biomedical

products. They have been preferred to organic antibiotics due to microbial resistance to organic products' continuous use [13]. The antimicrobial activity of these metal NPs may be related to several mechanisms including, the induction of oxidative stress due to the generation of reactive oxygen species (ROS), which may cause the degradation of the membrane structure of cell and release of ions from the NP's surface that has been reported to cause bacterial death due to binding to the cell membrane [14].

Besides, metal NPs can act to improve the mechanical and thermal properties of polymers. Recently, several studies on nanocomposite materials with biopolymer matrixes, such as cellulose-based polymers [15, 16], chitosan [17–20], polylactic acid (PLA) [21–23], and starch [24–27] have been reported. Recently, the interest in the PBAT is growing due to its flexibility and thermal properties, which are comparable to commodities plastics and so could be used in several areas. Moreover, the development of PBAT nanocomposites could enhance its properties for specific applications and make it economically competitive. Ferreira et al. investigated the addition of AgNPs-DDT (Dodecanethiol-protected silver nanoparticles) in the PBAT matrix and obtained nanocomposites with good mechanical performance and antifungal properties with a non-cytotoxic characteristic [28]. Luo et al. prepared PBAT nanocomposite films with nano-TiO_2 particles and observed that their mechanical and gas barrier properties significantly improved [29].

This study developed PBAT nanocomposite antibacterial films based on PBAT and ZnO and Ag-ZnO nanoparticles. Possible interactions between the nanofillers and the PBAT matrix were investigated, and the effects of the NPs on the mechanical, thermal, crystalline, and antibacterial properties against *Escherichia coli* of PBAT films.

Experimental

Materials

Poly(butylene adipate-co-terephthalate) (PBAT), under the tradename Ecoflex FS, with a mean molar mass of 66,500 $g.mol^{-1}$, was supplied by BASF Brazil. Zinc nitrate and silver nitrate were purchased from LabSynth, Brazil. Chloroform was purchased from Sigma-Aldrich (São Paulo, Brazil). *E. coli* was kindly supplied by Adolfo Lutz Institute (São Paulo, Brazil).

Materials

Nanoparticles preparation

According to the literature, zinc oxide (ZnO) nanoparticles and Zinc oxide doped with silver nanoparticles (AgNpZnO) were synthesized at the IPEN-USP laboratory. ZnO synthesis was carried utilizing water Mili-Q as a solvent, zinc nitrate as a metal precursor, and sodium hydroxide as a reductant agent [30]. The ZnO-Ag system was

synthesized utilizing the ZnO previously synthesized, Mili-Q water as the solvent, and silver nitrate as the metal precursor, and sodium citrate as reductant agent, the PVP was used as a core–shell agent [31]. The particles were centrifuged and washed to eliminate the other sub-products of the synthesis. After this process, the particles were dried in a dissecator until the total particles drying.

Films preparation

PBAT was previously dried at 50 °C for 24 h before use. Then, 20 g of PBAT was dissolved in 100 ml of chloroform with constant magnetic stirring. The polymeric solution was then applied to the glass plate (13 × 18 cm) and extended in film form using a wire extender TKB Erichsen (200 µm). The plates on which the wet polymer layer was deposited were subjected to one minute of air drying for solvent evaporation (flash-off). Then, the plates were immersed in distilled water to perform a coagulation bath. The films detached from the surface of the glass plates and were dried at room temperature.

For nanocomposites, ZnO and ZnO-Ag powders were incorporated after the PBAT solubilization in two different contents: 0.5 and 1 wt.%. According to the literature, the selected contents were determined; Dehghani et al. reported that nanometals' addition of up to 1% improves the mechanical properties of polymeric films [8].

Characterization

Transmission electron microscopy

The samples' morphology was examined with a JEOL JEM-2100 transmission electron microscope operating at a voltage of 80 kV.

Fourier-transform Raman spectroscopy

The spectra were collected using FT-Raman equipment (MultiRaman, Bruker Optics), equipped with a 1064 nm wavelength and 100 W power laser. The data acquisition was carried out in the range 600–4000 cm^{-1}, and 32 scans were collected with a resolution of 4 cm^{-1}.

Fourier-transform infrared spectroscopy

FTIR spectra were recorded on VARIAN 66 spectrophotometer (Perkin Elmer), and the samples were scanned using reflectance from 4000 to 500 cm^{-1}. A total of 32 scans were collected with a resolution of 4 cm^{-1}.

Mechanical properties

The films were evaluated by tensile tests according to ASTM D638-14, using an equipment Instron, model 3367 (Norwood, USA), with a load cell of 50 N and a test speed of 50 mm/min.

Field emission scanning electron microscopy and energy-dispersive spectroscopy

The samples were fixed in the specimen holder and coated with a thin layer of gold (10 nm). The samples were analyzed using a scanning electron microscope equipped with a chemical microanalysis module (EDS) using a working distance of 12 mm and a voltage of 15 keV. The analysis was performed to evaluate the elements C, O, Zn, and Ag.

Thermogravimetric analysis

The TGA was conducted on an equipment STA 6000 (PerkinElmer, USA), using alumina pans. The samples were heated from 30 to 600 °C at the heating rate of 10 °C min^{-1} under an N_2 atmosphere (flow rate of 20 mL min^{-1}).

Differential scanning calorimetry

Enthalpic properties of specimens were reported using a Mettler Toledo DSC 822^e differential scanning calorimeter. The thermal program used for polymer nanocomposite films was: step heating from − 30 to 220 °C at a heating rate of 10 °C min^{-1} under a nitrogen atmosphere; step holding for 5 min at − 30 °C, step cooling to − 10 °C, and step reheating to 220 °C at 10 °C min^{-1}.

X-ray diffraction

X-ray diffraction (XRD) measurements were carried out in the reflection mode on a diffractometer Rigaku Multiflex, (Tokyo, Japan), graphite monochromator, 40 kV, 20 mA, X-rays tube, copper anode $\lambda Cuk\alpha = 15418$ Å, scanning 2θ, from 3° to 60°, speed 0.06°/4 s, fixed time.

Antibacterial properties

Microbiological test was carried out with the inoculation of peace's of 1 × 1 cm films, in a 90 mm Petri dishes in a nutrient agar culture medium, inoculated with a suspension of the species' bacteria *E. coli* with a count of 10^5 colony-forming unit (CFU).ml^{-1}. After 48 h of inoculation in a microbiological oven at 37 °C, the inhibition radius was analyzed to evaluate the biocidal effect.

Results and discussion

Nanoparticles characterization

Transmission electron microscopy

Transmission electron microscopy results (Fig. 1) show that the ZnO-Ag nanoparticles (NPs) exhibited spherical morphology and diameters of approximately 50 nm.

The NPs indicate both Ag and ZnO, where the Ag is attached to the spherical ZnO surface but smaller. Kyomuhimbo et al. observed similar results in their work [32].

Fourier-transform Raman spectroscopy

The Raman spectroscopy indicates the vibrational mode activity of each nanoparticle, considering its chemical structure. Figure 2 presents the Raman spectra, and strong peaks of ZnO nanoparticles were found at 440, 724, 927, 1069, 1385, and 1405 cm^{-1}, attributed to the wurtzite ZnO nanocrystals formation [33]. Specifically, the peak 440 cm^{-1} is associated with Zn–O stretching, commonly found for ZnO particles [34]. Single crystalline ZnO belongs to the C_{6v} symmetry group with eight optical phonon modes in the Brillouin zone [35].

The ZnO-Ag nanostructure showed changes in peak intensity and location, associated with the Ag vibration modes and charge complexes that alter the Raman peaks [33]. The shift of peak 440–431 cm^{-1} indicates compressive stress in the crystal, which probably occurred due to the stress generated during the ZnO-Ag nanoparticle synthesis. The Ag can also induce defects such as interstitial Zn and oxygen vacancies in ZnO [36, 37] since the Ag nanoparticles probably are located around the ZnO-NPs, as illustrated in Fig. 3.

Films characterization

Chemical interactions–FTIR and FT-raman

FTIR and FT-Raman were used to analyze possible changes in the films' chemical structure after adding the ZnO and ZnO-Ag nanoparticles (NPs). The measurements are complementary; the FTIR spectra result from the electromagnetic radiation absorption or transmission by the sample, while the Raman spectrum is the result of spreading radiation over a specific wavelength (1064 nm) [38].

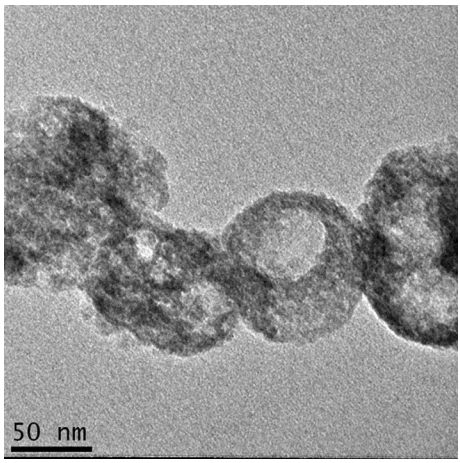

Fig. 1 TEM micrograph ZnO/Ag

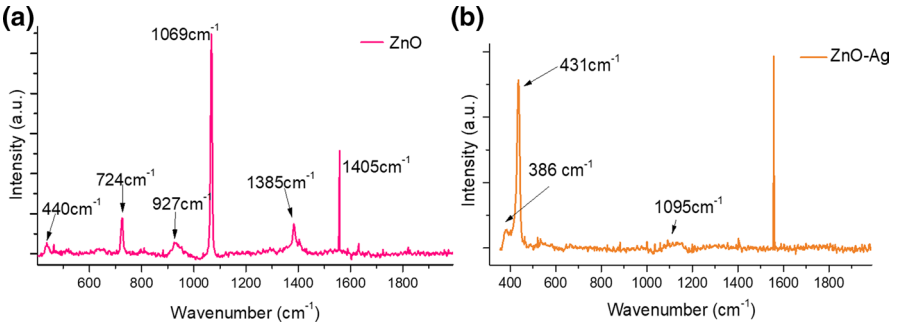

Fig. 2 Raman spectra of **a** ZnO and **b** ZnO-Ag nanoparticles

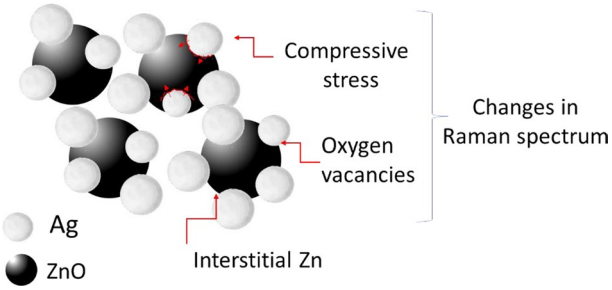

Fig. 3 Illustrative scheme of the ZnO-Ag nanoparticles, considering the ZnO as a carrier for the Ag-NPs

Figure 4 displays the FTIR spectra of PBAT and its films containing ZnO and ZnO-Ag. The main PBAT peaks observed in the FTIR spectrum included 2957, 1700, 1460, 1417, 1384, 1255, 1161, 1097, 1016, 935, 878, and 729 cm^{-1}, and these peaks are associated with CH_3 and CH_2 stretching, CH_2 in-plane bending mode, C-O stretching, =C-H and C=O bending mode of benzene ring [39, 40]. With the ZnO (Fig. 4a) or ZnO-Ag (Fig. 4b) addition, no new peaks or changes in the molecular frequencies were observed, which means that the NPs do not have intermolecular interactions with PBAT films.

Unlike observed in FTIR, the FT-Raman spectra showed differences between PBAT films without and with nanoparticles, and these variations can be associated with different vibration modes. Figure 5 shows the Raman spectra obtained for the neat PBAT film and containing ZnO (Fig. 5a) and ZnO-Ag (Fig. 5b).

The prominent PBAT peaks in Raman spectra were observed at 3085, 2927, 1719, 1621, 1454, 1287, 1090, 845, and 629 cm^{-1}, assigned to CH_2 and CH_3 vibration, C=C and C=O stretching, O-CH_2 bending mode, =C-H in the benzene ring, and out-plane =C-H bending mode [41, 42]. In the PBAT-ZnO spectra (Fig. 5b), an increase in peaks' intensity was observed at ~ 2927, 1454, and 1287 cm^{-1}, indicating physical interactions between the matrix and the NPs [43].

After the addition of ZnO-Ag nanoparticles, the spectra wholly changed. The vibrational frequencies show a shift in some peaks by 3–9 cm^{-1} [44]. The peaks

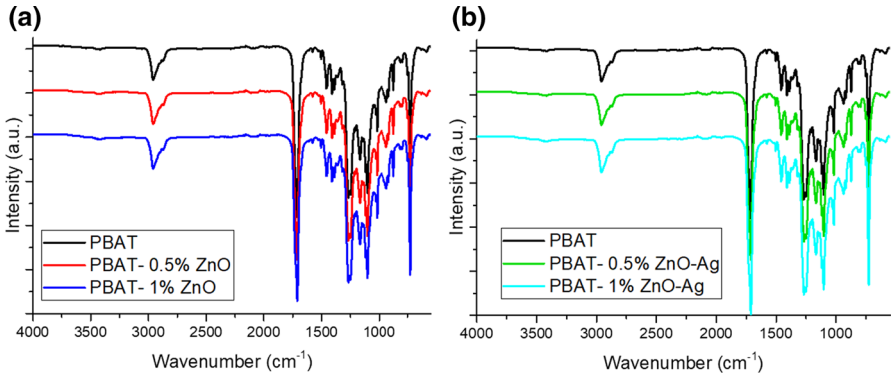

Fig. 4 FTIR spectra of PBAT and **a** PBAT-ZnO, and **b** PBAT-ZnO-Ag films

associated with vibrational frequencies of aromatic ring vibrations changed due to intermolecular interactions between the PBAT and ZnO-Ag. These significative changes are associated with the new molecular vibration of the matrix and the NPs in the films during excitation, suggesting a strong interaction between the mixture components.

Mechanical properties

Table 1 presents the mechanical results in terms of elastic modulus, tensile strength, and elongation at break. The pristine PBAT showed a stiffness of ~ 59 MPa, and ε of ~ 360%, which is coherent with those reported in the literature [29, 43]. The addition of ZnO or ZnO-Ag 0.5% increases the ε values and decreases the σ; this decrease is associated with the low nanoparticle content, which did not significantly change the polymer properties [2]. Low NPs contents could contribute to the films' flexibility without changing the material's stiffness, as verified in this work.

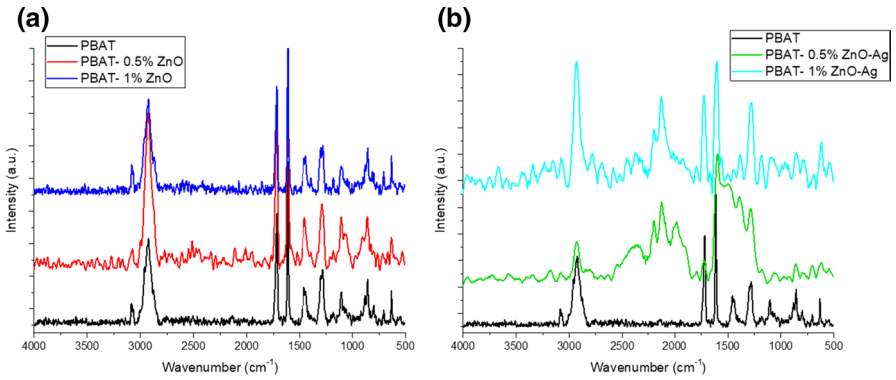

Fig. 5 Raman spectra of PBAT films without and with **a** ZnO, and **b** ZnO-Ag

Table 1 Mechanical properties of PBAT and its films: elastic modulus (E), tensile strength (σ), and elongation at break (ε)

Sample	E (MPa)	σ (MPa)	ε (%)
PBAT	59.1 ± 6.7	6.7 ± 1.9	358.9 ± 2.2
PBAT-0.5% ZnO	60.5 ± 5.0	6.1 ± 1.0	395.0 ± 1.5
PBAT-1% ZnO	65.5 ± 4.8	6.8 ± 1.3	354.3 ± 9.1
PBAT-0.5% ZnO-Ag	57.6 ± 5.8	5.7 ± 0.6	393.4 ± 0.3
PBAT-1% ZnO-Ag	80.7 ± 7.8	8.4 ± 1.3	394.6 ± 3.3

Table 2 Compositional analysis of PBAT and its films through SEM–EDS

Sample	C (wt.%)	O (wt.%)	Zn (wt.%)	Ag (wt.%)
PBAT	68.84	31.16	0	0
PBAT-0.5% ZnO	69.38	30.45	0.17	0
PBAT-1% ZnO	68.64	31.08	0.28	0
PBAT-0.5% ZnO-Ag	67.88	32.01	0.02	0.09
PBAT-1% ZnO-Ag	68.06	31.55	0.06	0.33

The addition of 1% NPs improved the stiffness, tensile strength, and elongation at break of the films; these increases, mainly observed for PBAT-1% ZnO-Ag, are indicative of homogeneous dispersion of the fillers in the PBAT matrix, with no agglomeration, compared to PBAT-1% ZnO film [8]. The physical interaction between ZnO-Ag and PBAT matrix, verified by FT-Raman spectroscopy, could beneficially transfer the stress, resulting in improved σ, and producing a hardening PBAT film [43].

Compositional analysis

The SEM–EDS was performed to evaluate the chemical elements present in the films qualitatively, and Table 2 shows the results. All the films contained similar amounts of carbon and oxygen, consistent with the PBAT structure composition. A small percentage of Zn confirmed the ZnO nanoparticle's inclusion within film structure, i.e., 0.17 and 0.28 wt.% of Zn for the PBAT-0.5% ZnO and PBAT-1% ZnO, respectively, confirming nanoparticles' presence in the film. Moreover, the percentage was lower than the NPs weight due to oxygen in ZnO composition and possible dispersion during film preparation. A similar trend was observed for films containing ZnO-Ag nanoparticles, with a higher concentration of nanoparticle incorporated, resulting in a higher quantity of Zn and Ag detected. It is highlighted that films containing ZnO-Ag presented a considerably higher amount of Ag than Zn, which possibly indicates that the Ag particles allocate at the ZnO surface.

Thermal analysis

Figure 6 shows the PBAT and its nanocomposites' thermogravimetric curves. The pristine polymer presents a typical single mass loss event associated with the

polymeric chains' scission in random regions between adipic acid and 1,4-butanediol within polymer structure [45]. The ZnO particles' films exhibited a decrease of ~ 50 °C in the T_{onset} temperature, associated with the ZnO catalytic activity under heat [46, 47].

The PBAT ZnO-Ag films showed good thermal stability without significant changes in the thermal degradation profile, which can be attributed to the NPs good dispersion, which decreases the oxygen permeability through the films. The "zigzag path" created by the nanoparticles delays the volatile components' scape, contributing to the films' thermal stability [44]. The thermal stability of ZnO-Ag NPs may result from silver protection around zinc since there is a significant difference in the oxidation potential between metals, and the Ag reduces the Zn oxidation capacity.

The films were also analyzed by differential scanning calorimetry, and Fig. 7 shows the second heating curves. The T_m values slightly decreased for PBAT-ZnO films, indicating that the nanoparticles can slightly hinder degradation kinetics [43].

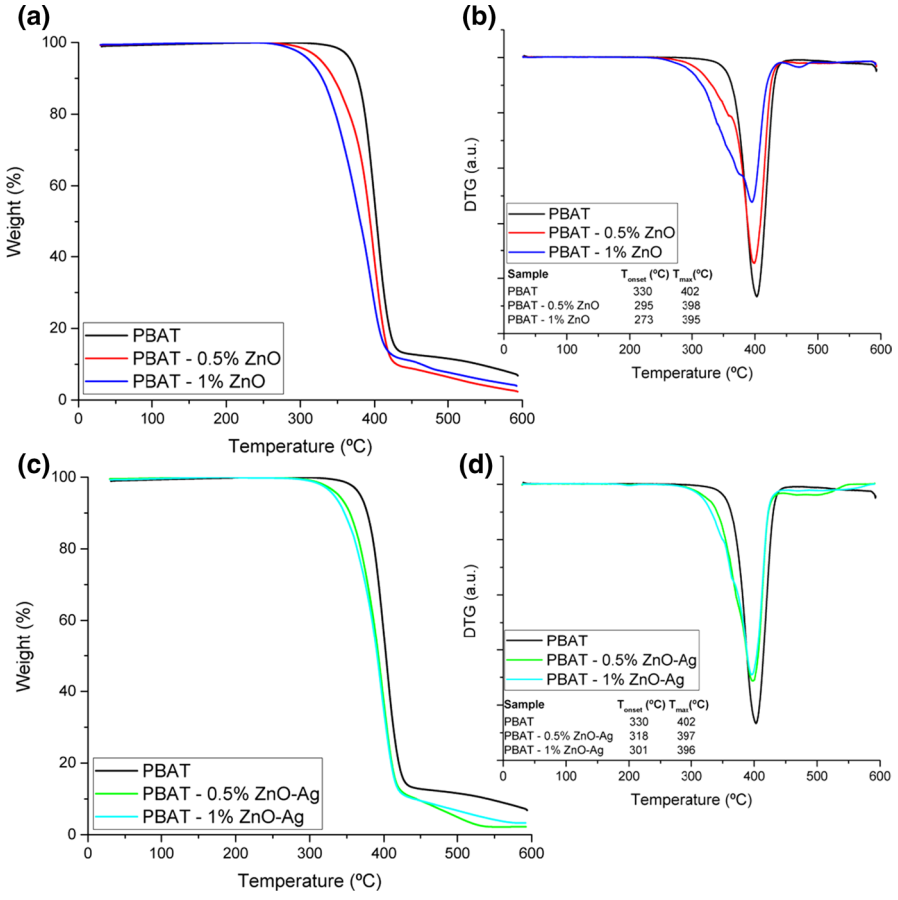

Fig. 6 Thermogravimetric curves for developed films with **a** TGA and **b** DTG for PBAT and ZnO films, and **c** TGA and **d** DTG for PBAT and ZnO-Ag films

However, the ZnO-Ag particles showed the opposite thermal behavior, with a slight increase in T_m values, indicating that the NPs can increase the polymer crystallinity.

X-ray diffraction

Figure 8 presets the diffractograms of NPs and the developed films. The ZnO NPs usually present a hexagonal wurtzite structure, as discussed in the Raman section, with very sharp diffraction peaks [48]. However, as observed in Fig. 8, the ZnO presented broadband without any typical diffraction peak due to the present water within the nanoparticle structure, which hinders the crystalline structure [49]. Calcination is usually applied in order to remove residual water and enhance the NPs crystallinity [50]. For the ZnO-Ag NPs, the multiple peaks are related to the ZnO and Ag structure, and the peaks at 31.4°, 34.4°, 36.2° can be assigned for (100), (002), (101) diffraction planes of ZnO structure [51, 52]. The Ag face-centered cubic structure showed peaks at 39.6° and 44.3° can be indexed to the (100) and (101) planes of the Ag [53].

The PBAT films presented a broad pattern, typical for semicrystalline polymers, with peaks at 16.2°, 17.4°, 20.2°, 23.1° and 24.8° typical of PBAT crystal structure [45]. These peaks were maintained for composites containing ZnO and ZnO-Ag, without significant changes in the diffraction pattern, i.e., the addition of the nanoparticles did not significantly change the polymer chains' organization.

The Crystallinity Index (CI) was calculated to evaluate the impact of NPs in film structure, considering the crystalline and amorphous contribution [54], and Table 3 shows the CI values. The pristine PBAT presents a small CI (18%), while the ZnO and the ZnO-Ag presented higher CI, evidencing the NPs high crystalline structure. Besides, the inclusion of NPs increased the film CI, proportionally with its concentration. More crystalline polymers have superior mechanical properties, as shown above, and modify the polymeric chains' availability for possible microbiological attacks. Microorganisms tend to preferentially attack the amorphous regions of the

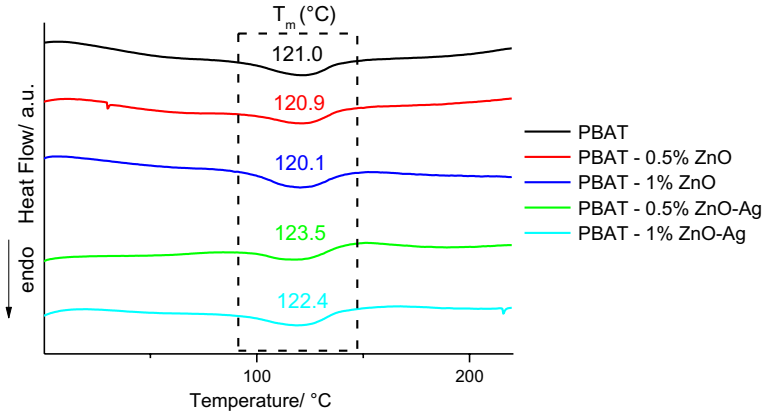

Fig. 7 DSC thermograms of PBAT films and its nanocomposites

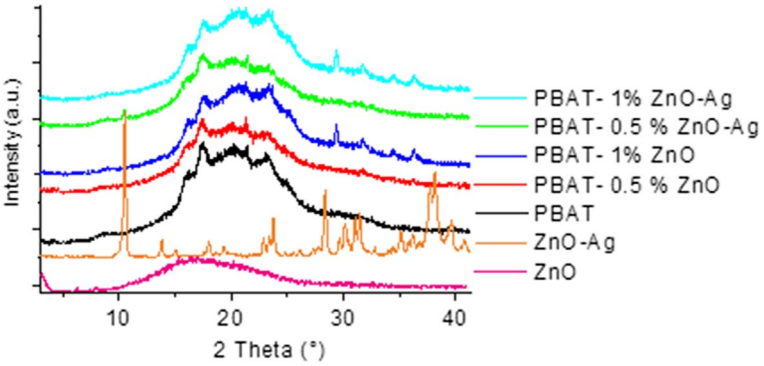

Fig. 8 X-ray diffractograms of the raw materials and PBAT films containing the ZnO and ZnO-Ag nanoparticles

carbon chain due to the higher disorganization degree, while the crystalline structures tend to remain intact for longer. Thus, the high crystallinity, mainly observed for PBAT—ZnO-Ag films, allows us to infer that the films are less susceptible to bacterial attacks, which was later confirmed and presented in the antimicrobial results.

Antibacterial properties

In this study, the PBAT films were tested for antimicrobial activity using *E. coli* (Gram-negative bacteria) as a foodborne pathogen, and Fig. 9 shows the obtained results. The *E. coli* is a high resistant microorganism due to its intrinsic membrane structure, which has a peptidoglycan layer and an outer membrane consisting of lipopolysaccharides and phospholipids, challenging to destroy [55]. The pristine PBAT (Fig. 9a) exhibited no antimicrobial activity, and although *E. coli* may not present specific enzymes for the PBAT chain degradation, the bacterium could grow using the film as a substrate, as indicated with red arrows.

The inclusion of ZnO-0.5% reduced the bacteria growth in the PBAT films; however, this effect was still observed (Fig. 10b). For ZnO-1% (Fig. 10c), the bacteria

Table 3 Crystallinity Index of nanoparticles, PBAT, and its films

Sample	Crystallinity index (%)
PBAT	17.9
ZnO	27.5
ZnO-Ag	56.1
PBAT-0.5% ZnO	18.8
PBAT-1% ZnO	22.9
PBAT-0.5% ZnO-Ag	22.6
PBAT-1% ZnO-Ag	27.5

was inhibited entirely within the film region, which probably occurred by the ZnO biological activity, that under visible light irradiation, generates Zn^{2+} ions that interact with microbial cells, resulting in the destruction of bacterial cell integrity and the generation of reactive oxygen species (ROS), such as H_2O_2, OH^-, and O_2^{-2} [12, 56]. The ROS may cause oxidative stress of bacterial cells, leading to *E. coli* death [6, 57]. Besides, the metal oxide can mechanically damage the bacteria cell, and the great surface area of the nanoparticles leads to a more intense effect [43, 58].

The PBAT ZnO-Ag films (Fig. 10d and e) showed antimicrobial properties even at lower NPs content, preventing *E. coli* growth. The silver addition enhanced the biocidal effect, probably due to the synergic antibacterial effect of ZnO-Ag nanoparticles. The Ag^+ has a spectral bactericidal action and can interact with bacterial cells' protein and nucleic acid, promoting ROS release and leading to cell damage. Also, silver ions can bind with phosphates, thiols, and hydroxyls, compromising respiration processes [13, 59].

The combination of ZnO and Ag nanoparticles increases the antimicrobial properties. At the zinc oxide surface, occur a re-deposition of metallic Zn from Zn^{2+} dissolved during the nanoparticle's formulation. Additionally, the Zn^0 may form from the reduction of oxide film itself, following equation: $ZnO + H_2O + 2e^-$ à $Zn + 2OH^-$. At this surface, the silver nanoparticles allocate, and thus the ZnO acts as Ag-carrier. Evaluating the oxidation–reduction potential, the standard reduction potential of Zn/Zn^{2+} is -0.76 V, while the standard reduction potential for Ag/Ag^+ is $+0.80$. The metallic Zn oxidates preferentially, protecting the metallic Ag from oxidation during storage, which helps stabilize the Ag nanoparticle and preserve its

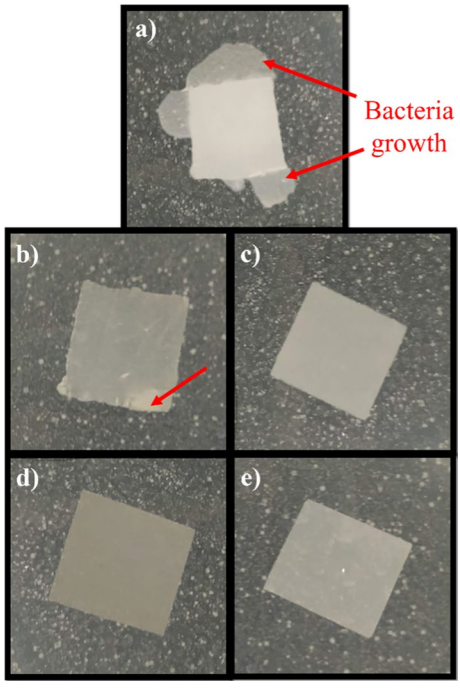

Fig. 9 Antimicrobial results against *E. coli* for **a** PBAT, **b** PBAT-0.5% ZnO, **c** PBAT-1% ZnO, **d** PBAT-0.5% ZnO-Ag, **e** PBAT-1% ZnO-Ag, with an indication with red arrows of bacteria growth within film region

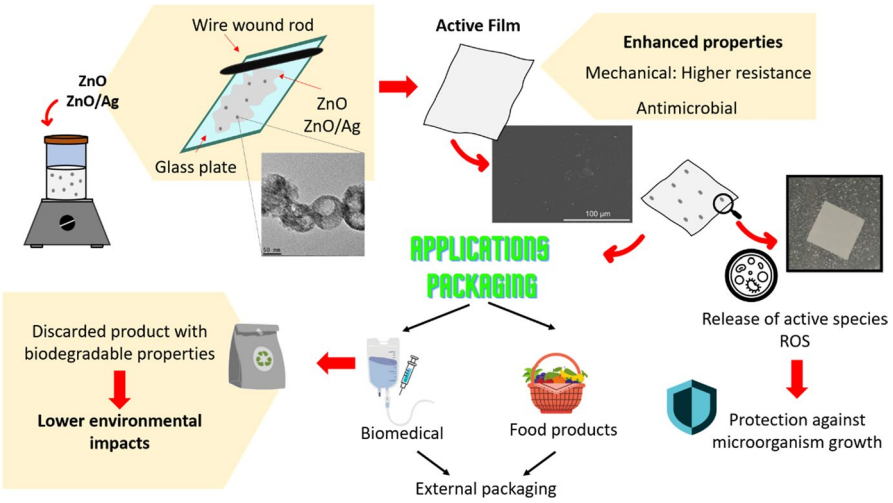

Fig. 10 Schematic illustration of film development, highlighting its enhanced properties, potential applications, and environmental aspects for using biodegradable materials

properties. As the particles enter in contact with the cellular wall of microorganisms, the Zn^{2+} acts directly, and the Ag^0 oxidates and release Ag^+ enhances the antimicrobial activity of the nanoparticles, resulting in a more significant antimicrobial effect with lower concentrations of NPs.

The results indicated that PBAT ZnO-Ag films have great potential as packaging for numerous antimicrobial applications, such as biological films and food packaging, as indicated in Fig. 10. The antimicrobial film market has shown a trend in the nanoparticles use to increase the biological and mechanical performance of polymeric films. Besides, there is a high consumer acceptance of nanoparticles since they are internationally recognized as safe for human health at low levels, as long as there is no migration to the packaged product [12, 59]. The biodegradable nanocomposites developed in this work showed superior biological and mechanical performance, potentially for antimicrobial applications.

Conclusions

In this work, poly(butylene adipate-co-terephthalate) (PBAT) films filled with ZnO and ZnO-Ag nanoparticles (NPs) were prepared. The NPs presented a spherical morphology and characteristic vibrational modes for wurtzite ZnO, with shifts promoted due to Ag-ZnO binding. The films presented the typical characteristics bands for PBAT structure, and the FT-Raman showed peaks that suggested interactions between nanoparticles and the matrix. Additionally, the NPs enhanced the mechanical properties, with substantial increases of Young Modulus, from 59 to 81 MPa for the samples PBAT and PBAT-1% ZnO-Ag. The thermal properties showed the typical curve observed for PBAT, with similar degradation behavior, and indicated that

NPs could increase the polymer crystallinity, corroborated with diffraction curves and the crystallinity index (CI). The CI values increased from 17.9% for the pristine PBAT to 27.5% for PBAT-1% ZnO-Ag. Antibacterial results showed that the PBAT matrix has no inhibition for *E. coli*. With the inclusion of 0.5 wt% ZnO NPs, the bacteria growth was reduced, and at 1 wt%, the bacterium was inhibited. The addition of ZnO-Ag resulted in complete inhibition of *E. coli*, showing that ZnO's combination with Ag presented a synergic effect due to ZnO acting as an Ag carrier, helping to stabilize it, increasing its efficiency. These results show promising results for antimicrobial applications like packages and biomedical products.

Acknowledgements The authors thank the financial support provided by FAPESP (2018/11277-7), CNPq, CAPES (Process No 88882.333460/2019-1), and the Multiuser Experimental Center of the Federal University of ABC (CEM-UFABC).

References

1. Venkatesan R, Rajeswari N (2019) Preparation, mechanical and antimicrobial properties of SiO_2 / poly(butylene adipate-co-terephthalate) films for active food packaging. SILICON 11:2233–2239. https://doi.org/10.1007/s12633-015-9402-8
2. Venkatesan R, Rajeswari N (2017) ZnO/PBAT nanocomposite films: investigation on the mechanical and biological activity for food packaging. Polym Adv Technol 28:20–27. https://doi.org/10.1002/pat.3847
3. Tavares LB, Ito NM, Salvadori MC, dos Santos DJ, Rosa DS (2018) PBAT/kraft lignin blend in flexible laminated food packaging: peeling resistance and thermal degradability. Polym Test 67:169–176. https://doi.org/10.1016/j.polymertesting.2018.03.004
4. Cardoso LG, Pereira Santos JC, Camilloto GP, Miranda AL, Druzian JI, Guimarães AG (2017) Development of active films poly (butylene adipate co-terephthalate)–PBAT incorporated with oregano essential oil and application in fish fillet preservation. Ind Crops Prod 108:388–397. https://doi.org/10.1016/j.indcrop.2017.06.058
5. Piedade AP, Pinho AC, Branco R, Morais PV (2020) Evaluation of antimicrobial activity of ZnO based nanocomposites for the coating of non-critical equipment in medical-care facilities. Appl Surf Sci 513:145818. https://doi.org/10.1016/j.apsusc.2020.145818
6. Kaushik M, Niranjan R, Thangam R, Madhan B, Pandiyarasan V, Ramachandran C, Oh DH, Venkatasubbu GD (2019) Investigations on the antimicrobial activity and wound healing potential of ZnO nanoparticles. Appl Surf Sci 479:1169–1177. https://doi.org/10.1016/j.apsusc.2019.02.189
7. Lule ZC, Kim J (2021) Compatibilization effect of silanized SiC particles on polybutylene adipate terephthalate/polycarbonate blends. Mater Chem Phys 258:123879. https://doi.org/10.1016/j.matchemphys.2020.123879
8. Dehghani S, Peighambardoust SH, Peighambardoust SJ, Hosseini SV, Regenstein JM (2019) Improved mechanical and antibacterial properties of active LDPE films prepared with combination of Ag, ZnO and CuO nanoparticles. Food Packag Shelf Life 22:100391. https://doi.org/10.1016/j.fpsl.2019.100391
9. Gao Z, Van Nostrand JD, Zhou J, Zhong W, Chen K, Guo J (2019) Anti-listeria activities of linalool and its mechanism revealed by comparative transcriptome analysis. Front Microbiol. https://doi.org/10.3389/fmicb.2019.02947
10. Li J, Ye F, Lei L, Zhao G (2018) Combined effects of octenylsuccination and oregano essential oil on sweet potato starch films with an emphasis on water resistance. Int J Biol Macromol 115:547–553. https://doi.org/10.1016/j.ijbiomac.2018.04.093
11. Khan A, Huq T, Khan RA, Riedl B, Lacroix M (2014) Nanocellulose-based composites and bioactive agents for food packaging. Crit Rev Food Sci Nutr 54:163–174. https://doi.org/10.1080/10408398.2011.578765
12. Kim I, Viswanathan K, Kasi G, Sadeghi K, Seo J (2020) ZnO Nanostructures in active antibacterial food packaging: preparation methods, antimicrobial mechanisms, safety issues, future prospects,

and challenges ZnO nanostructures in active antibacterial food packaging: preparation methods, antimicrobial. Food Rev Int 00:1–29. https://doi.org/10.1080/87559129.2020.1737709
13. Rai M, Yadav A, Gade A (2009) Silver nanoparticles as a new generation of antimicrobials. Biotechnol Adv 27:76–83. https://doi.org/10.1016/j.biotechadv.2008.09.002
14. Emamifar A (2011) Applications of antimicrobial polymer nanocomposites in food packaging. In: Haschim A (ed) Advanced Nanocomposite Technology. IntechOpen, Croatia
15. Khalil HA, Bhat AH, Yusra AI (2012) Green composites from sustainable cellulose nanofibrils: a review. Carbohydr Polym. https://doi.org/10.1016/j.carbpol.2011.08.078
16. Yu HY, Yao JM (2016) Reinforcing properties of bacterial polyester with different cellulose nanocrystals via modulating hydrogen bonds. Compos Sci Technol 136:53–60. https://doi.org/10.1016/j.compscitech.2016.10.004
17. Kumar S, Mukherjee A, Dutta J (2020) Chitosan based nanocomposite films and coatings: emerging antimicrobial food packaging alternatives. Trends Food Sci Technol. https://doi.org/10.1016/j.tifs.2020.01.002
18. Moustafa H, Youssef AM, Darwish NA, Abou-Kandil AI (2019) Eco-friendly polymer composites for green packaging: Future vision and challenges. Compos Part B Eng 172:16–25. https://doi.org/10.1016/j.compositesb.2019.05.048
19. Kohsari I, Shariatinia Z, Pourmortazavi SM (2016) Antibacterial electrospun chitosan–polyethylene oxide nanocomposite mats containing bioactive silver nanoparticles. Carbohydr Polym. https://doi.org/10.1016/j.carbpol.2015.12.075
20. Grząbka-Zasadzińska A, Amietszajew T, Borysiak S (2017) Thermal and mechanical properties of chitosan nanocomposites with cellulose modified in ionic liquids. J Therm Anal Calorim 130:143–154. https://doi.org/10.1007/s10973-017-6295-3
21. Ahmed J, Mulla M, Jacob H, Luciano G, Bini TB, Almusallam A (2019) Polylactide/poly(ε-caprolactone)/zinc oxide/clove essential oil composite antimicrobial films for scrambled egg packaging. Food Packag Shelf Life. https://doi.org/10.1016/j.fpsl.2019.100355
22. Dhar P, Bhasney SM, Kumar A, Katiyar V (2016) Acid functionalized cellulose nanocrystals and its effect on mechanical, thermal, crystallization and surfaces properties of poly (lactic acid) bionanocomposites films: a comprehensive study. Polymer (Guildf) 101:75–92. https://doi.org/10.1016/j.polymer.2016.08.028
23. Lin N, Huang J, Chang PR, Feng J, Yu J (2011) Surface acetylation of cellulose nanocrystal and its reinforcing function in poly(lactic acid). Carbohydr Polym 83:1834–1842. https://doi.org/10.1016/j.carbpol.2010.10.047
24. Olad A, Gharekhani H, Mirmohseni A, Bybordi A (2018) Superabsorbent nanocomposite based on maize bran with integration of water-retaining and slow-release NPK fertilizer. Adv Polym Technol 37:1682–1694. https://doi.org/10.1002/adv.21825
25. Patil MD, Patil VD, Sapre AA, Ambone TS, Torris AT, Shukla PG, Shanmuganathan K (2018) Tuning controlled release behavior of starch granules using nanofibrillated cellulose derived from waste sugarcane bagasse. ACS Sustain Chem Eng 6:9208–9217. https://doi.org/10.1021/acssuschemeng.8b01545
26. Pelissari FM, Andrade-Mahecha MM, do Amaral Sobral PJ, Menegalli FC (2017) Nanocomposites based on banana starch reinforced with cellulose nanofibers isolated from banana peels. J Colloid Interface Sci. https://doi.org/10.1016/j.jcis.2017.05.106
27. Peighambardoust SJ, Peighambardoust SH, Mohammadzadeh Pournasir N, Pakdel P (2019) Properties of active starch-based films incorporating a combination of Ag, ZnO and CuO nanoparticles for potential use in food packaging applications. Food Packag Shelf Life. https://doi.org/10.1016/j.fpsl.2019.100420
28. Ferreira FV, Mariano M, Lepesqueur LSS, Pinheiro IF, Santos LG, Burga-Sánchez J, Souza DHS, Koga-Ito CY, Teixeira-Neto AA, Mei LHI, Gouveia RF, Lona LMF (2019) Silver nanoparticles coated with dodecanethiol used as fillers in non-cytotoxic and antifungal PBAT surface based on nanocomposites. Mater Sci Eng C 98:800–807. https://doi.org/10.1016/j.msec.2019.01.044
29. Luo S, Zhang P, Gao D (2020) Preparation and properties of antimicrobial poly(butylene adipate-co-terephthalate)/TiO_2 nanocomposites films. J Macromol Sci Part B Phys 59:248–261. https://doi.org/10.1080/00222348.2020.1712045
30. Gusatti M, Rosário JA, Barroso GS, Campos CEM, Riella HG, Kunhen NC (2009) Synthesis of ZnO nanostructures in low reaction temperature. Chem Eng Trans 17:1017–1022. https://doi.org/10.3303/CET0917170

31. de Olyveira GM, Costa LM, de Carvalho AJ, Basmaji P, Pessan LA (2011) Novel LDPE/EVA nanocomposites with silver/titanium dioxide particles for biomedical applications. J Mater Sci Eng B 1(4B):516
32. Kyomuhimbo HD, Michira IN, Mwaura FB, Derese S, Feleni U, Iwuoha EI (2019) Silver–zinc oxide nanocomposite antiseptic from the extract of Bidens pilosa. SN Appl Sci 1:1–17. https://doi.org/10.1007/s42452-019-0722-y
33. Zamiri R, Rebelo A, Zamiri G, Adnani A, Kuashal A, Belsley MS, Ferreira JMF (2014) Far-infrared optical constants of ZnO and ZnO/Ag nanostructures. RSC Adv 4:20902–20908. https://doi.org/10.1039/c4ra01563k
34. Lefatshe K, Muiva CM, Kebaabetswe LP (2017) Extraction of nanocellulose and in-situ casting of ZnO/cellulose nanocomposite with enhanced photocatalytic and antibacterial activity. Carbohydr Polym 164:301–308. https://doi.org/10.1016/j.carbpol.2017.02.020
35. Mosquera E, Rojas-Michea C, Morel M, Gracia F, Fuenzalida V, Zárate RA (2015) Zinc oxide nanoparticles with incorporated silver: Structural, morphological, optical and vibrational properties. Appl Surf Sci 347:561–568. https://doi.org/10.1016/j.apsusc.2015.04.148
36. Mosquera E, Bernal J, Zarate RA, Mendoza F, Katiyar RS, Morell G (2013) Growth and electron field-emission of single-crystalline ZnO nanowires. Mater Lett 93:326–329. https://doi.org/10.1016/j.matlet.2012.11.119
37. Wang LN, Hu LZ, Zhang HQ, Qiu Y, Lang Y, Liu GQ, Ji JY, Ma JX, Zhao ZW (2011) Studying the raman spectra of Ag doped ZnO films grown by PLD. Mater Sci Semicond Process 14:274–277. https://doi.org/10.1016/j.mssp.2011.05.004
38. Rodrigues ADG, Galzerani JC (2012) Espectroscopia de IV, UV e raman. Rev Bras Ensino Física 34:4309
39. He X, Li P (2020) Surface water pollution in the middle chinese loess plateau with special focus on hexavalent chromium (Cr6+): occurrence, sources and health risks. Expo Heal. https://doi.org/10.1007/s12403-020-00344-x
40. Hernández-López M, Correa-Pacheco ZN, Bautista-Baños S, Zavaleta-Avejar L, Benítez-Jiménez JJ, Sabino-Gutiérrez MA, Ortega-Gudiño P (2019) Bio-based composite fibers from pine essential oil and PLA/PBAT polymer blend morphological, physicochemical, thermal and mechanical characterization. Mater Chem Phys 234:345–353. https://doi.org/10.1016/j.matchemphys.2019.01.034
41. Cai Y, Lv J, Feng J, Liu Y, Wang Z, Zhao M, Shi R (2012) Discrimination of poly(butylenes adipate-co-terephthalate) and poly(ethylene terephthalate) with fourier transform infrared microscope and raman spectroscope. Spectrosc Lett 45:280–284. https://doi.org/10.1080/00387010.2011.610420
42. Cai Y, Lv J, Feng J (2013) Spectral characterization of four kinds of biodegradable plastics: poly (lactic acid), poly (butylenes adipate-co-terephthalate), poly (hydroxybutyrate-co-hydroxyvalerate) and poly (butylenes succinate) with FTIR and raman spectroscopy. J Polym Environ 21:108–114. https://doi.org/10.1007/s10924-012-0534-2
43 Felipe Jaramillo A, Riquelme S, Montoya LF, Sánchez-Sanhueza G, Medinam C, Rojas D, Salazar F, Pablo Sanhueza J, Francisco Meléndrez M (2019) Influence of the concentration of copper nanoparticles on the thermo-mechanical and antibacterial properties of nanocomposites based on poly(butylene adipate-co-terephthalate). Polym Compos. https://doi.org/10.1002/pc.24949
44. Biswas MC, Jeelani S, Rangari V (2017) Influence of biobased silica/carbon hybrid nanoparticles on thermal and mechanical properties of biodegradable polymer films. Compos Commun 4:43–53. https://doi.org/10.1016/j.coco.2017.04.005
45. Barbosa RFS, Souza AG, Rosa DS (2020) Acetylated cellulose nanostructures as reinforcement materials for PBAT nanocomposites. Polym Compos. https://doi.org/10.1002/pc.25580
46. Wahid F, Duan YX, Hu XH, Chu LQ, Jia SR, Cui JD, Zhong C (2019) A facile construction of bacterial cellulose/ZnO nanocomposite films and their photocatalytic and antibacterial properties. Int J Biol Macromol 132:692–700. https://doi.org/10.1016/j.ijbiomac.2019.03.240
47. Zhou K, Gui Z, Hu Y, Jiang S, Tang G (2016) The influence of cobalt oxide-graphene hybrids on thermal degradation, fire hazards and mechanical properties of thermoplastic polyurethane composites. Compos Part A Appl Sci Manuf 88:10–18. https://doi.org/10.1016/j.compositesa.2016.05.014
48. Saboor A, Shah SM, Hussain H (2019) Band gap tuning and applications of ZnO nanorods in hybrid solar cell: Ag-doped verses Nd-doped ZnO nanorods. Mater Sci Semicond Process 93:215–225. https://doi.org/10.1016/j.mssp.2019.01.009

49. Senthilkumar SR, Sivakumar T (2014) Green tea (Camellia sinensis) mediated synthesis of zinc oxide (ZnO) nanoparticles and studies on their antimicrobial activities. Int J Pharm Pharm Sci 6:461–465
50. Venu Gopal VR, Kamila S (2017) Effect of temperature on the morphology of ZnO nanoparticles: a comparative study. Appl Nanosci. https://doi.org/10.1007/s13204-017-0553-3
51. Pascariu P, Cojocaru C, Samoila P, Airinei A, Olaru N, Rusu D, Rosca I, Suchea M (2020) Photocatalytic and antimicrobial activity of electrospun ZnO: Ag nanostructures. J Alloys Compd 834:155144. https://doi.org/10.1016/j.jallcom.2020.155144
52. Marimuthu T, Anandhan N, Thangamuthu R (2018) Electrochemical synthesis of one-dimensional ZnO nanostructures on ZnO seed layer for DSSC applications. Appl Surf Sci 428:385–394. https://doi.org/10.1016/j.apsusc.2017.09.116
53. Jung HJ, Koutavarapu R, Lee S, Kim JH, Choi HC, Choi MY (2018) Enhanced photocatalytic degradation of lindane using metal–semiconductor Zn@ZnO and ZnO/Ag nanostructures. J Environ Sci (China) 74:107–115. https://doi.org/10.1016/j.jes.2018.02.014
54. Saadiah MA, Zhang D, Nagao Y, Muzakir SK, Samsudin AS (2019) Reducing crystallinity on thin film based CMC/PVA hybrid polymer for application as a host in polymer electrolytes. J Non Cryst Solids 511:201–211. https://doi.org/10.1016/j.jnoncrysol.2018.11.032
55. Panthi G, Park SJ, Chung HJ, Park M, Kim HY (2017) Silver nanoparticles decorated Mn_2O_3 hybrid nanofibers via electrospinning: towards the development of new bactericides with synergistic effect. Mater Chem Phys 189:70–75. https://doi.org/10.1016/j.matchemphys.2016.12.026
56. Seray M, Skender A, Hadj-Hamou AS (2020) Kinetics and mechanisms of Zn2+ release from antimicrobial food packaging based on poly (butylene adipate-co-terephthalate) and zinc oxide nanoparticles. Polym Bull. https://doi.org/10.1007/s00289-020-03145-z
57. Gupta R, Das N, Singh M (2019) Fabrication and surface characterisation of c-ZnO loaded TTDMM dendrimer nanocomposites for biological applications. Appl Surf Sci 484:781–796. https://doi.org/10.1016/j.apsusc.2019.04.136
58. Zhang J, Cao C, Zheng S, Li W, Li B, Xie X (2020) Poly (butylene adipate-co-terephthalate)/magnesium oxide/silver ternary composite biofilms for food packaging application. Food Packag Shelf Life 24:100487. https://doi.org/10.1016/j.fpsl.2020.100487
59. Tri Handok C, Huda A, Gulo F (2019) Synthesis pathway and powerful antimicrobial properties of silver nanoparticle: a critical review. Asian J Sci Res. https://doi.org/10.3923/ajsr.2019.1.17.s